Hydrated Cs^+-Exchanged MFI Zeolites: Location and Population of Cs^+ Cations and Water Molecules in Hydrated $Cs_{6.6}$MFI from In and Ex Situ Powder X-ray Diffraction Data as a Function of Temperature and Other Experimental Conditions

Bernard F. Mentzen*

5 Rue Marcel Desplaces, F-69330 Meyzieu, France

Gérard Bergeret

IRC (Institut de Recherches sur la Catalyse), CNRS, 2 Avenue Albert-Einstein, F-69626 Villeurbanne, France

Hermann Emerich

SNBL (Swiss−Norwegian Beam Lines), ESRF (European Synchrotron Radiation Facility), 6 Rue Jules-Horowitz, P.O. Box 220, F-38043 Grenoble, France

Hans-Peter Weber

ACCE, F-38960 St Aupre, France, and LCr/IPMC/BSP, Swiss Federal Institute of Technology, CH-1015 Lausanne, Switzerland

Received: March 28, 2006; In Final Form: May 10, 2006

Extending our previous investigation of dehydrated, Cs-exchanged MFI zeolites (*J. Phys. Chem. B* **2006**, *110*, 97−106) to hydrated analogues, we have determined the crystal structures of members of the $Cs_{6.6}H_{0.3}$-MFI·xH_2O series, for $0 < x < 28$, from synchrotron-radiation powder diffraction data. In the fully hydrated phase, three independent Cs^+ cations and six water molecules are identified in difference Fourier maps. The populations of the cations amount to 2.79/3.40/0.41 Cs/unit cell (uc) for the Cs1/Cs2/Cs3 sites, respectively, and those of the water molecules to 4/4/4/4/8/4 H_2O/uc for the Ow1/Ow2/Ow3/Ow4/Ow5/Ow6 sites, respectively. Close to water saturation, the Cs3 and Ow6 sites are near each other (∼1.44 Å) and are not occupied simultaneously. At saturation, Cs cations and water molecules form three interconnected $Cs(H_2O)_n$ clusters and one $(H_2O)_4$ cluster in the MFI channel system: $Cs2(H_2O)_5$ centered at $x/y/z \sim -0.018/0.146/0.546$ (midway between the intersection and the straight channels), $Cs1(H_2O)_4$ centered at ∼0.056/0.240/0.889 (the zigzag channel openings), $Cs3(H_2O)_2$ centered at ∼0.228/0.25/0.899 (in the zigzag channel), and the $(H_2O)_4$ cluster (in the zigzag channel) bonded to Cs1 and Ow1. $(H_2O)_4$ and $Cs3(H_2O)_2$ exclude each other. The $Cs2(H_2O)_5$ clusters are connected through weak Ow5···Ow5′ hydrogen bonds (2.88 Å) and form polymeric chains in the straight channel direction (010). During progressive hydration this Cs2 cation enlarges its hydration shell, stepwise, from $Cs2(H_2O)_2$ to $Cs2(H_2O)_3$, to $Cs2(H_2O)_4$, and finally to a $Cs2(H_2O)_5$ cluster. During the dehydration process, these extraframework species migrate, and it is shown that for varying total H_2O/uc loadings the individual populations of the Cs^+ cations and H_2O molecules strongly depend on experimental and measurement (in situ vs ex situ) conditions. The shapes of the channels change also; except for $T > 150$ °C, in all the $Cs_{6.6}H_{0.3}$MFI·xH_2O phases, the straight channel D10R (double 10-ring) pore openings ($1.16 < \epsilon < 1.23$) become strongly elliptical. The framework structure of all the investigated phases conforms to orthorhombic *Pnma* space group symmetry. Hydration and dehydration in $Cs_{6.6}$MFI are fully reversible processes. From a knowledge of the Cs^+ locations, we are able to estimate, by computer simulations, the positions of H_2O molecules in $Cs_{6.6}H_{0.3}$MFI·$28H_2O$. The maximum theoretically possible water loading in an hypothetical and idealized cationless $[Cs_{6.6}H_{0.3}]$MFI structure amounts to 48 H_2O/uc (nine independent water species), which is in fair agreement with existing high-pressure data (47 H_2O/uc). This value is to be compared with the water saturation capacity obtained in a structural refinement of sealed-tube diffraction data of a proton-exchanged $H_{6.9}$MFI·$38H_2O$ (seven independent water molecules). In the crystal structure of this H−ZSM-5 phase, the straight channel openings are almost circular ($\epsilon = 1.08$). From this we conclude that the main factor responsible for the flexibility of the MFI framework is the presence of the $Cs(H_2O)_n$ clusters residing in, or close to, the straight channel double 10-rings.

1. Introduction

Zeolites[1] are microporous crystalline aluminosilicates that have applications in three major areas: sorption, ion exchange, and catalysis (see ref 1 for our previous work on this topic). Their anionic framework consists of a network of corner-sharing TO_4 tetrahedra. These T atoms are occupied mostly by tetravalent Si(IV) and trivalent Al(III) but often also by other elements such as T = Ge(IV), Ti(IV), Al(III), B(III), Ga(III), Fe(III), P(V), and even Li(I).[2] Because of the charge imbalance caused by the presence of non-tetravalent atoms (for instance, one charge per Al(III)/unit cell (uc)), protons (H^+) or metallic cations (e.g., Li^+, Na^+, K^+, Rb^+, Cs^+, Ca^{2+}, Ba^{2+}, Cu^+, Cu^{2+}, Ag^+, Tl^+, Ni^{2+}, or Co^{2+}) are used to compensate for the negative charges introduced. These compositional and structural

* Author to whom correspondence should be addressed. E-mail: mentzen.b@infonie.fr.

10.1021/jp061909s CCC: $33.50
Published on Web 06/27/2006

TABLE 1: Pore Diameters and Largest Possible Sorbates in FAU,[3a] LTA,[3a] and MFI[3a−d] Zeolites

openings (T-ring)	maximum free diameter (Å)	zeolite and T-ring type	largest sorbate (Å)
6T[a]	2.8	FAU: S6R (sodalite cage)	H_2O (2.7), NH_3 (2.6)
8T	∼3.0, 3.8, 4.5	LTA: 3A, 4A, 5A − S8R	H_2O (2.7), CO_2 (3.3)
10T	5.5	MFI: D10R	*p*-xylene (8.0 × 4.3)
12T	7.4	FAU: S12R (super-cage)	1,3,5-mesithylene (7.3)

[a] T is the number of corner-sharing TO_4 tetrahedra in the ring. S6R, S8R, D10R, and S12R represent single 6-ring, single 8-ring, double 10-ring, and single 12-ring, respectively.

features alone suffice to convey to this class of materials exceptional qualities that render them indispensable for the applications mentioned above. The size and shape of the cavities in the framework govern the properties of zeolites as absorbents. This size and shape selectivity, combined with the easy exchangeability of the charge-compensating extraframework cations, in turn make zeolites matchless ion exchangers. Finally, the high thermal stability of the aluminosilicate framework, together with the three characteristics just mentioned, account for the extraordinary appeal of zeolites in heterogeneous catalysis. The wide variety of cage volume and opening sizes available, together with a cation palette ranging from H^+ to Ba^{2+}, permits one to custom-tailor the catalytic and molecular sieving properties of zeolites to the task at hand. Some examples showing the influence of selective cation exchange (in LTA-type[3a] zeolites) and of pore-opening sizes on some sorption properties in LTA-, FAU-,[3a] and MFI-type[3a−d] zeolites are given in Table 1.

In this paper, the second of a series (see ref 1), we continue to focus on accurately locating simple cations and representative guest molecules, as a function of temperature and other experimental conditions, in one of the two industrially most important zeolite structures: MFI (the other one being FAU). This series of papers on structural characteristics of MFI-type materials has the advantages of commonality of material origin, experimental technique, analytical approach, and investigators.

While the basic structural features of MFI are known,[3a−d] the exact location of extraframework cations, water, and other molecules, particularly under working conditions, often remains a matter of conjecture, left to guesstimates. One even finds cases where the information on these locations is described as being in a chaotic state.[4] The dearth of such essential information is a testimony to the difficulty of the experiment; it is painstaking, time-consuming work, with few immediate rewards. That a complete structural description is a prerequisite to fully understand any solid-state process, at both the experimental and the theoretical levels, is a truism. And yet we still find examples where extensive computer-modeling on MFI-type materials has been carried out based on scanty structural information. Because of their chemical composition ($0 < Al/uc < 10$, usually only 3−5) MFI-type materials contain fewer acid sites per unit cell than faujasites, and this is expected to yield flat, almost featureless landscapes of the electric potential across the cavities.[5] Consequently, the number of sites that are able to attract and bond exchangeable charge-compensating cations is low and difficult to detect. This is one of the reasons why, as of this date, structural investigations aimed at locating cations in MFI-type materials (termed silicalite for $Si/Al > 150$ and ZSM-5 for Si/Al lower than 100) are rather scarce and have not yet been rewieved.[6] Despite some former attempts to localize cations in ZSM-5 materials,[7−11] no cationic positions have been determined unambiguously until the recent study of a Cs-exchanged and fully dehydrated Cs−ZSM-5 phase.[12] This highly unsatisfactory situation prompted us to initiate a comprehensive investigation devoted to the cation and water locations in cation-exchanged M−ZSM-5 materials (M = Na^+, K^+, Rb^+, Cs^+, Tl^+, Cu^+, Cu^{2+}, Ba^{2+}, and possibly H^+ and Li^+). We hope to answer some of the following general questions: (a) Where are the extraframework cations located and what are their relative populations, (b) do the locations of the extraframework species depend on the experimental conditions, and if yes, which ones, (c) are these locations and populations similar in as-is hydrated samples, in dehydrated phases, or in rehydrated phases, (d) where do the cations relocate to in the presence of sorbed polar (e.g., water) or nonpolar (e.g., benzene or *p*-xylene) molecules, (e) which are the migrating species, the cations, the sorbates, or both, (f) is it possible to predict the locations of the sorbed water molecules by computer simulations, and finally, (g) how is the framework symmetry (possible solid-state phase transitions, existence of multiphase domains) and/or its flexibility (creation of elliptical D10R (double 10-ring) pore openings) affected by the cations and/or the nature of the sorbed molecules?

Our first paper[1] reported on Cs^+ locations, populations, and migrations as a function of temperature in previously thermally dehydrated Cs_xMFI phases ($0.7 < x < 7.7$ Cs/uc). It revealed the existence of five distinct cation sites over the whole range of Cs exchange, thus answering questions a and b and partially g. The present paper deals with locations and relocations of Cs^+ cations and water molecules during progressive thermal dehydration in an initially fully hydrated $Cs_{6.6}H_{0.3}MFI{\cdot}28H_2O$ sample. We have started with the Cs^+ cation instead of lighter cations such as H, Li, or K because (1) the probability to detect this electron-rich cation in difference Fourier (DF) maps (after partial structure refinements using X-ray powder diffraction techniques) is high, (2) Cs-exchanged ZSM-5 phases are currently investigated in computer simulations and adsorption studies,[13,14−17] and (3) the location(s) of this cation can be used to model the preferred sites of other cations in theoretical studies.[18,19]

The paper is organized as follows. Section 2 deals with experimental conditions and analytical methodology. Section 3 presents the results obtained experimentally, first for the completely hydrated starting phase, then for the several phases obtained in the ensuing dehydration process, performed both in situ and ex situ. Results from a computer simulation of the water molecule locations are presented in section 4. In section 5 we compare and discuss our results, and in section 6 we finally draw our conclusions.

2. Experimental Section

The starting Cs-exchanged ZSM-5 material investigated in the present work corresponds to the eighth sample listed in Table 1 of ref 1. In its totally dehydrated form, the unit-cell content of this sample has the chemical formula of $Cs_{6.6}H_{0.3}Al_{6.9}Si_{89.1}O_{192}$ (in short $Cs_{6.6}H_{0.3}$MFI). The experimental setups used at the Swiss−Norwegian Beam Lines (Grenoble, France; BM01B) and at the Institut de Recherches sur la Catalyse (Villeurbanne, France) as well as the analytical tools used (Rietveld method using modified DBW[20] code and the EXPGUI[21] package) are also the same as those reported in ref 1.

In its totally hydrated form, the investigated MFI-type material has the $Cs_{6.6}H_{0.3}MFI{\cdot}28H_2O$ composition (obtained by thermogravimetry, water adsorption isotherms, and chemical analysis). The structural changes occurring during progressive thermal dehydration of this $Cs_{6.6}H_{0.3}MFI{\cdot}28H_2O$ zeolitic material are investigated under two different experimental protocols. In the

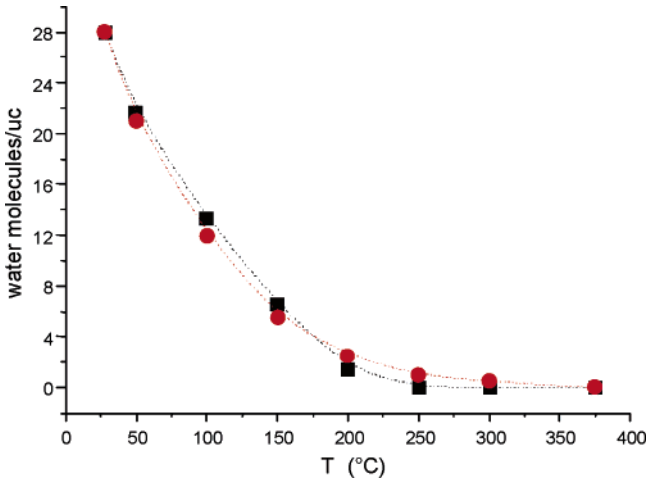

Figure 1. Dehydration of $Cs_{6.6}H_{0.3}MFI{\cdot}28H_2O$ as observed by thermogravimetry: circles, observed values; squares, Rietveld-refined values.

first one, a series of samples, termed hyd_1 HT, are examined in situ. Under this protocol a single sample is packed into an open quartz capillary and mounted on the temperature- and atmosphere-controlling equipment assembled at the SNBL. From room temperature (28 °C), the temperature is progressively ramped up, in 50 °C increments, to several plateaus (i.e., 50, 100, 150, 200, 250, 300, and exceptionnally, 375 °C) and maintained there for at least 20 min before a diffraction pattern is collected. Dehydration equilibrium is considered as achieved when the intensity of the first intense diffraction peak is constant. In a second series, termed hyd_2 RT, the samples are characterized ex situ. According to this protocol, eight glass capillaries are filled with $Cs_{6.6}H_{0.3}MFI{\cdot}28H_2O$ and progressively preheated in a small furnace. At selected temperatures T_1 (45, 63, 85, 109, 136, 176, 225, and 281 °C), one capillary after the other is then sealed, one at a time, slowly cooled to ambient temperature, and stored afterward for at least 1 week prior to data collection. Under these preparation conditions, the exact water/uc content does not correspond to that predicted from interpolation of the preheating temperature (T_2) on the thermogravimetry curve (Figure 1). Indeed, the time gap between removal of the capillary from the furnace and its sealing (safety match + epoxy adhesive) as well as the unavoidable dead volume in the capillary after sealing are not negligible. And, of course, the actual water/uc contents are known only after the structure refinements. The diffraction measurements for these ex situ samples, corresponding to the hyd_2 RT series, were also performed at the SNBL, using synchrotron radiation with $\lambda = 0.79991$ Å.

To obtain the hydrated H-form corresponding to the $Cs_{6.6}H_{0.3}MFI{\cdot}28H_2O$ phase, its parent zeolite (in the as-is Na-MFI form) is at first repeatedly NH_4-exchanged in 0.2 M ammonium nitrate solutions. After thermal calcination at 550 °C and total rehydration, the resulting $H_{6.9}MFI{\cdot}38H_2O$ phase is investigated at room temperature by X-ray powder diffraction (Cu Kα radiation, Panalytical X'Pert Pro MPD diffractometer, X'Celerator Panalytical detector).

The computer simulation method (molecular mechanics (MM)) used for predicting the water locations in the actual evacuated $Cs_{6.6}H_{0.3}MFI$ structure and in a hypothetical, strictly cationless MFI phase presenting the identical framework structure (maximum possible water loadings in a cationless framework) is detailed in ref 1. The potential parameters of the Cs^+ cations and of the T(Si,Al),O atoms are those used previously[1] in the MFI structure, and those of the water molecules are given in ref 22.

3. Results from Diffraction Experiments

3.1. Structure of $Cs_{6.6}H_{0.3}MFI{\cdot}28H_2O$ at Room Temperature (26 °C). The starting MFI framework parameters of the totally hydrated $Cs_{6.6}H_{0.3}MFI{\cdot}28H_2O$ phase are those reported in ref 1 for its dehydrated $Cs_{6.6}H_{0.3}MFI$ form (*Pnma* space group symmetry). Once the framework structure has been refined, the DF maps reveal the presence of extraframework residues that can be attributed to both Cs^+ and water sites (Figure 2). These three Cs^+ cation sites and six water sites are then incorporated into the structural model, and the Rietveld refinement is completed. As discussed in ref 1, the total cesium content is constrained to its chemical formula value (6.6 Cs/uc). Plots of the powder diffraction patterns are shown in Figure 3.

The cesium populations refined for the Cs1/Cs2/Cs3 sites are 2.79(3)/3.40(1)/0.41(1) Cs/uc, respectively. At the early stages of the refinement, the water/uc populations for the Ow1/Ow2/Ow3Ow4/Ow5/Ow6 sites converged toward 0.47(2)/0.51(1)/0.62(3)/0.48(2)/0.98(2)/0.46(5), respectively. The maximum population of a site close to the *Pnma* mirror plane (*m*) is 4/uc. To avoid, as much as possible, split sites and undesired structural correlations, the *y*-coordinates of the water molecules that are close to *m* are fixed to $^1/_4$, and their maximum population to 4 molecules/uc. Experimental details and final refined atomic coordinates for the Si and O atoms are reported in Tables 2 and 3, respectively. Coordinates of the Cs cations and water molecules are reported separately in Table 4. The thermal parameters for the Si, O, and Cs atoms are those given in ref 1. For the water molecules, the global thermal parameter is fixed at $U_{iso} = 0.125$ Å^2. A detailed diagram of the refined $Cs_{6.6}H_{0.3}MFI{\cdot}28H_2O$ crystal structure is given in Figure 4. The ellipticity (ratio between the longer and the shorter O···O diameters of the elliptic channel section) of the straight channel pore opening is $\epsilon = 1.164$.

Figure 5 gives a schematic view of the $Cs_{6.6}H_{0.3}MFI{\cdot}28H_2O$ structure, where the connections between the Cs cations and the water molecules are highlighted. The three Cs cations and the six water molecules form three interconnected $Cs(H_2O)_n$ clusters and one $(H_2O)_4$ cluster in the MFI channel system: $Cs2(H_2O)_5$ centered at $x/y/z \sim -0.018/0.146/0.546$ (midway between the intersection, site I, and the straight channels, site III), $Cs1(H_2O)_4$ centered at ~0.056/0.240/0.889 (the zigzag channel openings), $Cs3(H_2O)_2$ centered at ~0.228/0.25/0.899 (in the zigzag channel, site II), and the $(H_2O)_4$ cluster (in the zigzag channel) bonded to Cs1 and Ow1. $(H_2O)_4$ and $Cs3(H_2O)_2$ exclude each other. The $Cs2(H_2O)_5$ clusters are connected through weak Ow5···Ow5 = 2.88(5)Å hydrogen-bonded water molecules and form polymeric chains in the straight channel *b*-axis direction. All these clusters share one or more water molecules. The environments of the cations and water molecules are reported in Table 5. In the dehydrated $Cs_{6.6}H_{0.3}MFI$ form the shortest Cs−O distances between the cations and the framework oxygen atoms are 3.37(1)/3.33(5)/3.34(8)/3.08 Å for Cs1/Cs2/Cs3/Cs3′, respectively. In the hydrated form, only Cs1 has short Cs1−O26 = 3.35(2) Å and Cs1−O17 = 3.38(1) Å distances. The Cs2 and Cs3 cations have moved from their locations in the dehydrated phase (by 1.74 and 0.4 Å, respectively) to form the $Cs2(H_2O)_5$ and $Cs3(H_2O)_2$ clusters. The cation locations in the dehydrated and the fully hydrated phases are compared in Figure 6: After hydration of the $Cs_{6.6}H_{0.3}MFI$ phase, the Cs2′ and Cs3′ cations are replaced by the Ow5 and Ow2 molecules, respectively. The Cs2 cation, which is the most hydrated one (coordinating five water molecules), relocates toward the center of the intersection (a 1.74 Å shift), and all its former interactions with the framework are dramatically weak-

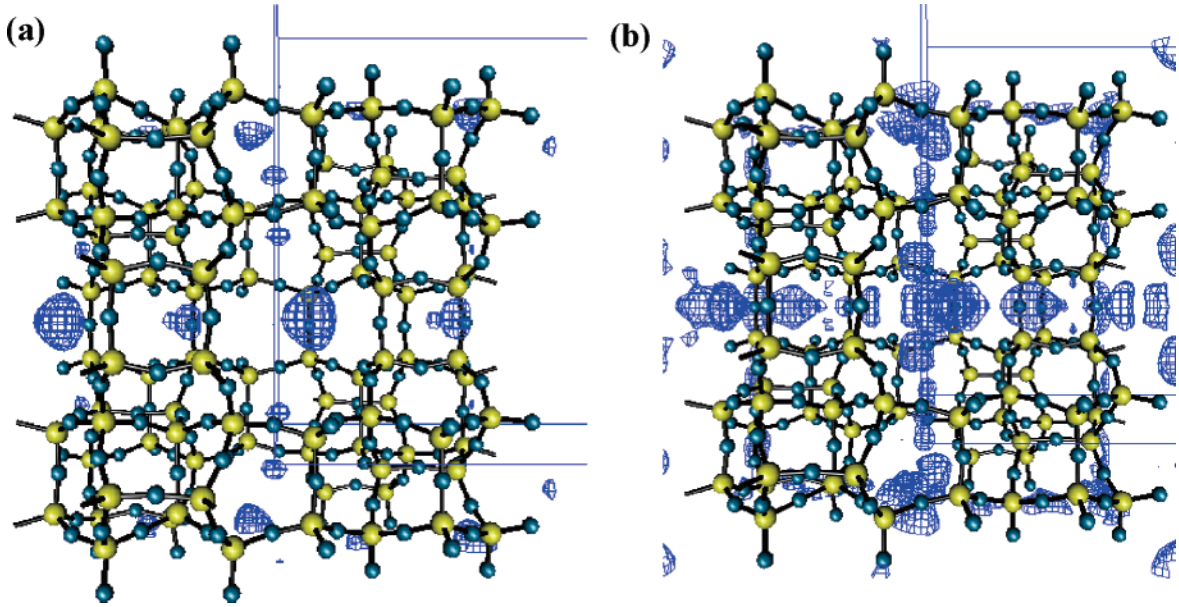

Figure 2. Three-dimensional DF maps showing the extraframework species in (a) the dehydrated $Cs_{6.6}H_{0.3}MFI$ and (b) the hydrated $Cs_{6.6}H_{0.3}MFI{\cdot}28H_2O$ phases.

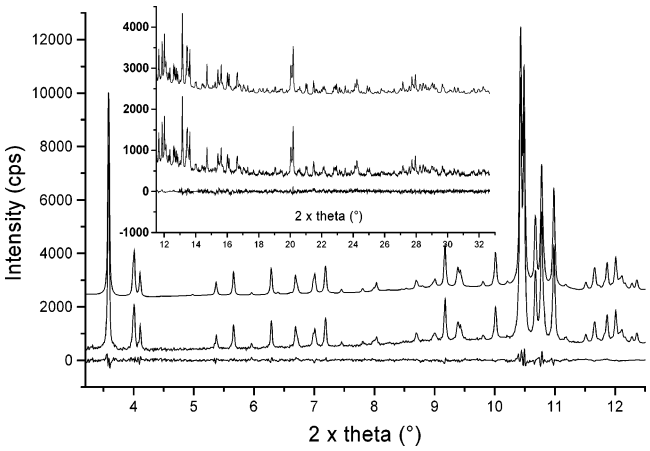

Figure 3. X-ray diffraction pattern of the fully hydrated $Cs_{6.6}H_{0.3}MFI{\cdot}28H_2O$ phase at room temperature: calculated (upper trace), observed (middle trace), and difference (lower trace) profiles.

ened. Cs3 has moved ~0.4 Å from its location in the dehydrated zeolite (the Cs3−O20 = 3.34(8) Å distance in $Cs_{6.6}H_{0.3}MFI$ is now 3.72(1) Å in the hydrated phase).

3.2. Dehydration of the $Cs_{6.6}H_{0.3}MFI{\cdot}28H_2O$ Phase As Observed In Situ at Increasing Temperatures (28−281 °C). The experimental conditions for the data collection of the dehydrated $Cs_{6.6}H_{0.3}MFI{\cdot}28H_2O$ phases in the hyd_1 HT series and the methods of crystal structure refinement are described in sections 2 and 3.1, respectively. Figure 1 shows the thermogravimetric curve corresponding to the dehydration of $Cs_{6.6}H_{0.3}MFI{\cdot}28H_2O$. It is evident from the curve that the differences between experimental and refined water/uc loadings are rather small (~1 H_2O). Figure 7a represents the evolutions, at increasing temperature, of the individual Cs/uc populations as a function of total Cs/uc content as obtained after the Rietveld-type structure refinements. In this figure, the first and the last data points correspond to the hydrated phase at 28 °C section 3.1) and the dehydrated phase at 450 °C (ref 1), respectively. Figure 7b shows the corresponding population for the dehydrated phase (ref 1). As already mentioned (section 3.1), in the hydrated $Cs_{6.6}H_{0.3}MFI{\cdot}28H_2O$ zeolite, the Cs2′ and Cs3′ cation species have vanished; therefore, to compare Figures 7a and 7b, the (Cs2 + C2′)/uc and (Cs3 + Cs3′)/uc values corresponding to the dehydrated $Cs_{6.6}H_{0.3}MFI$ phase are merged into Cs2 and Cs3, respectively. The refined individual Cs/uc and water/uc values in the hyd_1 HT series are reported in Table 6, and the unit-cell parameters and straight channel ellipticities (ϵ) in Table 7. The evolutions of the individual Cs/uc and water/uc contents as a function of total water fillings are given in Figures 8 and 9.

TABLE 2: Experimental and Selected Crystallographic Parameters for the $Cs_{6.6}H_{0.3}MFI{\cdot}28H_2O$ Phase at Room Temperature (28 °C)

chemical formula	$Cs_{6.6}H_{0.3}Al_{6.9}Si_{89.1}O_{192}{\cdot}28H_2O$
space group	*Pnma*
powder diffractometer	SNBL BM01B beam-line, custom-built, 6 detectors with Si (111) monochromators
scan range (2θ, deg)	1.524−32.66
profile function (U, V, W, η)	pseudo-Voigt (4 parameters)
wavelengths (Å)	0.69918 (*hyd_1*) and 0.79991 (*hyd_2*)[a]
step size (2θ, deg)	0.004
counting time per step (s)	1
no. background points (linear interpolation)	53
no. of data points	7785
no. of contributing reflections (*hkl*)	1527
no. of refined structural parameters	162
a (Å)	20.0592(2)
b (Å)	19.9411(2)
c (Å)	13.4300(2)
$R_p/R_{wp}/R_{exp}/R(F^2)$ (%)	4.16/5.40/4.00/8.57
Si−O/O···O restraints (Å)	1.59/2.60 (~ideal T_d)
refined Si−O range (Å)	1.567−1.618 (*mean 1.593*)
N−P + C	7340
sample temperatures (°C) hyd_1 series[a]	28, 50, 100, 150, 200, 250, 300, 375
heating conditions	ambient pressure, regulated hot air gun
preheated samples (T_1 °C) hyd_2 series[a]	45, 63, 85, 109, 136, 176, 225, 281
(T_2 °C)	(34, 40, 50, 67, 100, 150, 164, 178)

[a] See Experimental Section.

3.3. Dehydration of the $Cs_{6.6}H_{0.3}MFI{\cdot}28H_2O$ Phase As Observed Ex Situ at Room Temperature (26 °C). Interpretation of the eight powder diffraction patterns corresponding to

TABLE 3: $Cs_{6.6}H_{0.3}MFI\cdot28H_2O$ at Room Temperature (28 °C)[a]

atom	*x*	*y*	*z*
T1	0.4239(2)	0.0594(2)	−0.3430(3)
T2	0.3060(2)	0.0329(2)	−0.1989(3)
T3	0.2814(2)	0.0594(2)	0.0231(3)
T4	0.1227(2)	0.0623(2)	0.0176(3)
T5	0.0706(2)	0.0315(2)	−0.1968(3)
T6	0.1834(2)	0.0600(2)	−0.3355(3)
T7	0.4214(2)	−0.1721(2)	−0.3352(3)
T8	0.3059(2)	−0.1266(2)	−0.1909(3)
T9	0.2769(2)	−0.1720(2)	0.0247(3)
T10	0.1890(2)	−0.1732(2)	0.0207(3)
T11	0.0681(2)	−0.1313(2)	−0.1933(3)
T12	0.1855(2)	−0.1714(2)	−0.3278(3)
O1	0.3687(3)	0.0601(4)	−0.2581(5)
O2	0.3076(4)	0.0598(4)	−0.0879(3)
O3	0.2017(1)	0.0584(4)	0.0233(6)
O4	0.1001(4)	0.0594(4)	−0.0954(3)
O5	0.1114(2)	0.0557(4)	−0.2889(4)
O6	0.2397(3)	0.0542(4)	−0.2544(5)
O7	0.3686(3)	−0.1558(4)	−0.2490(5)
O8	0.3062(4)	−0.1506(4)	−0.0788(3)
O9	0.1976(2)	−0.1591(4)	0.0264(6)
O10	0.0938(4)	−0.1583(4)	−0.0890(3)
O11	0.1131(3)	−0.1566(4)	−0.2828(5)
O12	0.2398(3)	−0.1505(4)	−0.2462(5)
O13	0.3096(4)	−0.0469(1)	−0.1912(6)
O14	0.0726(4)	−0.0501(1)	−0.1917(6)
O15	0.4206(3)	0.1287(3)	−0.4020(5)
O16	0.4082(4)	0.0001(3)	−0.4207(5)
O17	0.4032(4)	−0.1304(3)	−0.4322(4)
O18	0.1883(4)	0.1312(3)	−0.3887(5)
O19	0.1916(4)	0.0022(3)	−0.4155(5)
O20	0.1965(4)	−0.1281(3)	−0.4247(4)
O21	−0.0051(2)	0.0526(4)	−0.2051(5)
O22	−0.0071(2)	−0.1525(4)	−0.2066(5)
O23	0.4192(6)	−0.25	−0.3594(8)
O24	0.1925(6)	−0.25	−0.3531(8)
O25	0.2899(6)	−0.25	0.0425(8)
O26	0.1047(6)	−0.25	0.0466(8)

[a] For the Cs and water coordinates see Table 4. The T and O framework sites are fully occupied. U_{iso} (Å^2) of T/O = 0.0168(38)/0.024(9).

TABLE 4: Comparison between the Refined and Simulated Cs and Water Positions in the $Cs_{6.6}H_{0.3}MFI\cdot28H_2O$ Crystal Structure

	refined			atom/	simulated		
atom	*x*	*y*	*z*	uc	*x*	*y*	*z*
Cs1	0.0561(4)	0.2405(12)	0.8867(5)	2.79	0.0561	0.2405	0.8867[a]
Cs2	−0.0183(4)	0.1464(3)	0.5462(5)	3.40	−0.0183	0.1464	0.5462
Cs3	0.2277(7)	0.25	0.8987(15)	0.41	0.2277	0.25	0.8987
Ow1	−0.0006(4)	0.25	0.6915(7)	4(f)[a]	−0.0533	0.2419	0.7136
Ow2	−0.1506(5)	0.25	0.7059(17)	4(f)	−0.1300	0.2496	0.6674
Ow3	0.0379(13)	0.25	0.4188(15)	4(f)	0.0182	0.2511	0.4006[b]
Ow4	0.1498(5)	0.25	0.7169(10)	4(f)	0.0685	0.2515	0.6075
Ow5	0.0296(11)	−0.0025(5)	0.4024(9)	8(f)	0.0406	0.0507	0.4199
Ow6	0.2277(7)	0.1780(4)	0.8987(f)	4(f)	0.1432	0.1838	0.7807

[a] Fixed. [b] Predicted as a possible sixth Cs cation in ref 1. For Ow1/Ow2/Ow3/Ow4/Ow5 and Ow6 the distances (Å) between the refined and the simulated water locations are 1.1/0.7/0.5/2.2/0.9/2.3 Å, respectively. U_{iso} (Å^2) of Cs/Ow = 0.143(40)/0.13(1).

the room temperature hyd_2 RT series (preheated and sealed samples) is given in section 3.1. The refined Cs/uc and water/uc populations are given in Table 8, and the unit-cell parameters and the straight channel ellipticities (ϵ) in Table 9. The evolutions of the individual Cs/uc and water/uc concentrations versus total water loadings are represented in Figures 10 and 11, respectively. As described in the Experimental Section, the samples corresponding to the hyd_2 RT series are obtained by preheating them at several temperatures (T_1) and cooling them prior to the diffraction measurement. The actual water/uc contents in the sealed samples cannot be precisely predicted from simple interpolation on the thermogravimetry (TG) curve (Figure 1). It is the structure refinements that finally yield the actual total water/uc contents. By comparing them with the TG curve, one can estimate the corresponding equivalent temperature (labeled as T_2 in Tables 8 and 9).

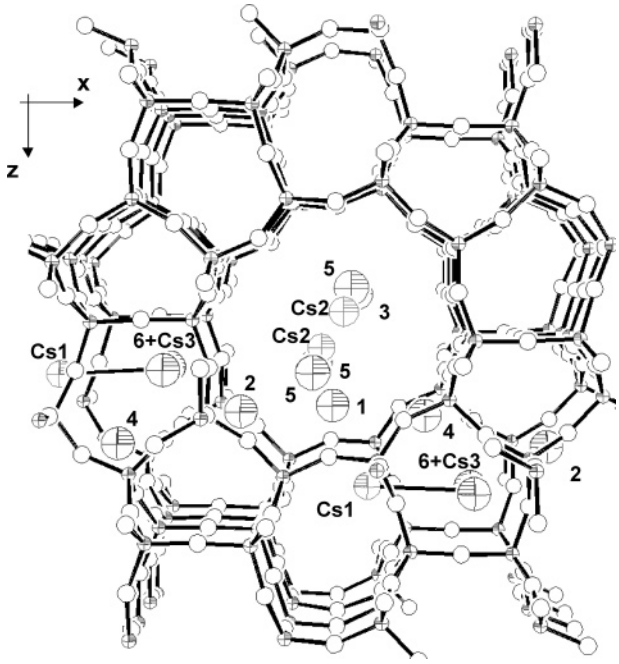

Figure 4. Detail of the $Cs_{6.6}H_{0.3}MFI\cdot28H_2O$ crystal structure showing the extraframewotk cesium cations (Cs1, Cs2, and Cs3) and the six water molecules (1, 2, 3, 4, 5, and 6). The sites corresponding to the Cs3 cation and Ow6 are not occupied simultaneously.

4. Results from Computer Simulations of Water Locations

In a previous simulation (ref 1) we have shown that the locations of the Cs^+ cations in the totally dehydrated $Cs_{6.6}H_{0.3}$-MFI phase could be correctly simulated. In this same simulation a sixth site was also predicted for cesium. It now appears that this site ought to be attributed instead to the terminal Ow3 water molecule, located close to the center of the channel intersection (site I). As related in section 3.1, the locations of the Cs1, Cs2, and Cs3 species in the hydrated $Cs_{6.6}H_{0.3}MFI\cdot28H_2O$ zeolite are very similar to some of those in the dehydrated one.

In the present simulation, the positions of the cations are held fixed, and only the locations of the water molecules are optimized by energy minimization as a function of increased water/uc loadings.

4.1. $Cs_{6.6}H_{0.3}MFI\cdot28H_2O$ Phase. The starting structural model used to predict the locations of the water molecules in the presence of the cesium cations corresponds to a spherical moiety (20 Å radius) of the actual $Cs_{6.6}H_{0.3}MFI$ framework. To prevent the energy-minimized water molecules from escaping the structural model, the outer openings of all the channel sections are blocked by crystallographically equivalent Cs^+ cations. In the simulation, the water molecules are added one by one, and their locations are alternatively optimized, at increasing water contents. Only six plausible water sites are simulated. Adding a seventh water molecule led to convergence toward chemically unrealistic Cs−water or water−water distances. Overall agreement between these computer-simulated water locations and those obtained from the structural refinements is fair to good, as judged from a numerical (Table 4) and a graphical (Figure 12) comparison. For some of the

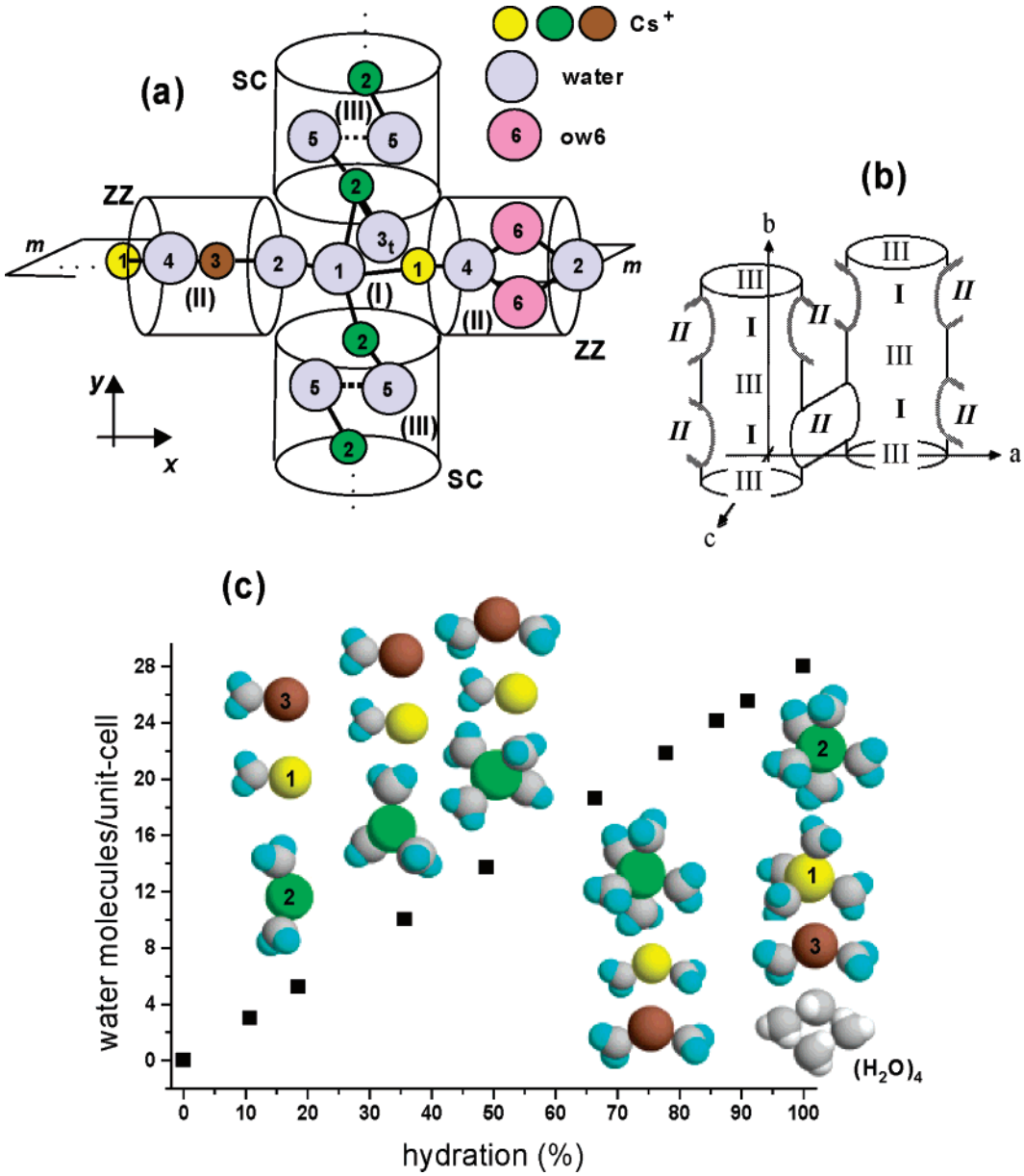

Figure 5. (a) Schematic view of the $Cs_{6.6}H_{0.3}$MFI·$28H_2O$ crystal structure showing the Cs1$(H_2O)_4$ (in the intersection, close to the zigzag channel opening), Cs2$(H_2O)_5$ (close to the straight channel opening), Cs3$(H_2O)_2$ (in the intersection zigzag channel), and $(H_2O)_4$ (in the zigzag channel) clusters. (Only Cs−O bonds corresponding to the first coordination sphere are represented.) Cs3$(H_2O)_2$ and $(H_2O)_4$ are mutually exclusive. 3t is a terminal water molecule that is not bonded to any of the other clusters. (b) Insert showing the MFI-type channel system and the labeling of the three characteristic I, II, and III absorption sites. (c) Clusters existing at five water loadings. The same color scheme applies to spherical atoms in parts a and c: green, yellow, brown, light gray, and cyan for Cs2, Cs1, Cs3, water oxygen, and hydrogen, respectively.

simulated water sites, the distances between calculated and refined positions are rather important: 1.1/0.7/0.5/2.2/0.9/ 2.3 Å for Ow1/Ow2/Ow3/Ow4/Ow5/Ow6, respectively. Such discrepancies, however, are not unusual in computer simulations using simple MM interaction models. These often neglect possible specific water−water and/or water−framework oxygen interactions as, for instance, hydrogen bonds or even the formation of genuine chemical bonds. The MM model, which is of the van der Waals type, is best suited for predicting starting refinement models, essentially based on geometric space-filling considerations, and this is also what we use our simulations for.

4.2. Idealized Cationless $Cs_{6.6}H_{0.3}$MFI Phase. Recently, it has been shown that at high pressure the water sorption capacity of a silicalite sample (a purely silicic MFI-type zeolite with Si/Al > 5000) is about 47 H_2O/uc.[23,24] Under normal atmospheric pressure conditions, the highly hydrophobic silicalite adsorbs only 4 H_2O/uc.[25] To estimate, by computer simulation, the maximum water sorption capacity of a strictly cationless MFI-type zeolite, which has the framework structure of $Cs_{6.6}H_{0.3}$-MFI (a purely hypothetical zeolitic material), we progressively filled it with several independent water molecules. The highest water/uc content attained in our simulation is 48 H_2O/uc, which is very close to the experimentally observed value[23,24] but far from a recently reported value (60 H_2O/uc)[26] obtained by computer simulations. The atomic coordinates of the nine independent water molecules and a schematic view of their distribution in the MFI channel system are given in Table 10 and Figure 13, respectively. The water molecules form polymeric chains constituted by corner- and base-sharing tetrahedra running in the *a*-axis direction; these chains are interconnected through the straight channels (in the *b*-axis direction) by dimeric $(H_2O)_2$ bridges.

TABLE 5: Selected Cation-to-Framework-Anion Bonds and Cation−Water, Water−Water, and Water−Framework Distances (Å) in the $Cs_{6.6}H_{0.3}$MFI·$28H_2O$ Phase at 28 °C[a]

atom pair	distance	atom pair	distance	atom pair	distance
Cs1−O15	3.52(1)	Cs2−O21	3.84(2)	Cs3−O24	3.70(2)
Cs1−O17	**3.38**(1)	Cs2−O5	3.86(2)	Cs3−O20	3.72(1)
Cs1−O23	3.45(1)				
Cs1−O26	**3.35**(2)				
Cs1−O4	3.72(1)				
Cs1−Ow1	**2.86**(3)	Cs2−Ow1	**2.86**(2)	Cs3−Ow2	**2.82**(3)
Cs1−Ow4	2.96(3)	Cs2−Ow3	**2.91**(2)	Cs3−Ow4	**2.90**(3)
Cs1−Ow6	3.66(3)	Cs2−Ow5	2.96(3)		
Cs1−Ow6	3.81(3)	Cs2−Ow2	3.99(3)		
		Cs2−Ow5′[b]	3.67(3)		
Ow1−Ow2	***3.01***(4)	Ow2−Ow6	3.16(4) × 2	Ow4−Ow6	3.23(3) × 2
Ow1−Ow3	3.74(3)	Ow5−Ow5	***2.88***(5)	Ow6−Ow6	***2.87***(5)
Ow2−O26	3.45(3)	Ow3−O7	3.48(2)	Ow4−O18	***2.87***(2)
				Ow4−O25	***2.64***(3)
Ow5−O1	3.18(3)	Ow6−O2	***2.86***(3)		
Ow5−O2	3.46(3)	Ow6−O3	2.96(3)		
Ow5−O5	3.38(3)	Ow6−O4	3.49(3)		
Ow5−O21	***2.87***(3)	Ow6−O6	3.22(3)		
		Ow6−O20	2.99(3)		

The Shortest Cation-framework or Cation−Water Distances Are in Bold Characters, and the Most Probable Hydrogen Bonds Are in Italics [a] Only distances less than 3.85 Å for Cs−O/Ow-Ow and 3.50 Å for Ow-O are given. [b] Ow5′ is the symmetry-related Ow5 site (through the inversion center).

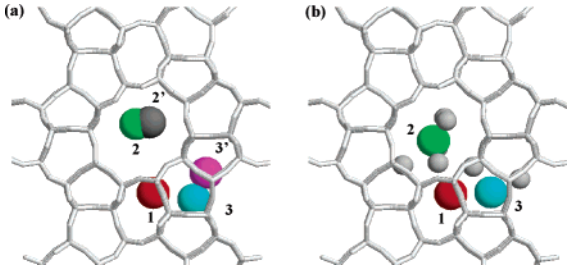

Figure 6. Cs cations (a) in $Cs_{6.6}H_{0.3}$MFI and (b) in $Cs_{6.6}H_{0.3}$MFI·$28H_2O$.

5. Discussion

By comparing the present fully hydrated phase with the dehydrated phase studied previously,[1] also investigated at room temperature, we notice that hydration leads to the relocation of only a few cations and that this migration must be attributed to the newly arising cation−water (a polar sorbate) interactions. This cation relocation concerns only Cs2 and Cs3; Cs1 is *not* shifted (maximum observed shift ~0.24 Å). This can be interpreted by assuming that of all the cations Cs1 is the one most involved in short Cs−framework interactions. In other words, this cationic site, bonded to the O17, O23, and O26 framework oxygen atoms, which in turn are bonded to possible Al-substituted Si T-sites, i.e., Si4 + Si7, Si4 × 2, and Si10 × 2, is proposed as a model for a potentially specific site in electric-field gradient (EFG) calculations.[5] This site is shown in Figure 5a by the small yellow circle labeled 1 (in the hydrated phase). The same site, which is comparable in both the dehydrated and the hydrated phases, is sketched in Figure 14. In the case of Cu(I)−ZSM-5 exchanged MFI-type materials, a similar site, labeled Z6(T10) (Al substituting Si10 of a *6*-ring in the zigzag channel) or 6T(T7−T11−T10−T10−T11−T7), is calculated by computer simulations for the location of the highly reactive Cu^+ ion.[27,28] In the case of a silver-exchanged Ag^+−ZSM-5 phase, an embedded quantum cluster model simulation predicts that the T7 site is a better candidate than

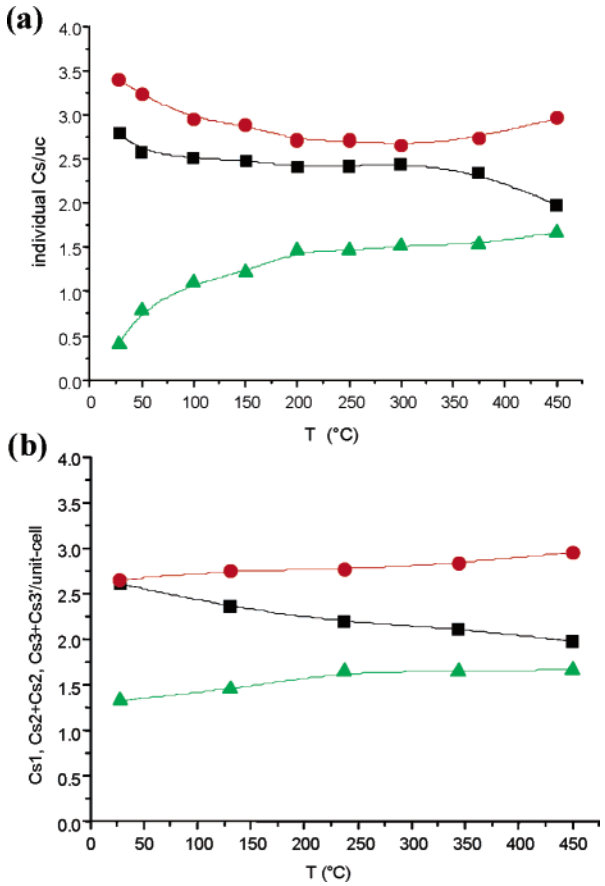

Figure 7. Populations of Cs sites as a function of temperature (a) in hydrated $Cs_{6.6}H_{0.3}$MFI·nH_2O and (b) in dehydrated $Cs_{6.6}H_{0.3}$MFI phases (see ref 1): squares, Cs1; circles, Cs2 (hydrated) or Cs2 + Cs2′ (dehydrated); triangles, Cs3 (hydrated) or Cs3 + Cs3′ (dehydrated). In both cases the total Cs/uc amounts to 6.6.

TABLE 6: Individual Cation and Water Populations (uc) in the hyd_1 HT Series[a]

T (°C)	Cs1	Cs2	Cs3	total water	Ow1	Ow2	Ow3	Ow4	Ow5	Ow6	*y*(Cs2)
28	2.79	3.40	0.41	28	4	4	4	4	8	4	0.1464(3)
50	2.58	3.23	0.79	22	4	4	4	4	5.7	0	0.1444(3)
100	2.51	2.95	1.10	14	1.3	3	3	4	3	0	0.1435(3)
150	2.48	2.88	1.22	6.6	0.5	1	0	2.9	2.2	0	0.0884(3)
200	2.41	2.71	1.46	1.5	0	0.1	0	1.4	0	0	0.0803(3)
250	2.42	2.71	1.46	0							0.0755(3)
300	2.45	2.65	1.52	0							0.0649(3)
375	2.35	2.74	1.53	0							0.0721(3)

[a] The esd's on the individual Cs/uc and water/uc contents are typically 0.02 and 0.1, respectively.

T12 for Si/Al substitution.[29] In the following sections, the results obtained by investigating the crystal structure of $Cs_{6.6}H_{0.3}$MFI·$28H_2O$, will be generalized to the study of the structural evolution of increasingly dehydrated phases measured either at progressively increased temperatures ($28 < T < 375$ °C; the hyd_1 HT series) or at room temperature (26°C; the hyd_2 RT series), after preheating.

5.1. Comparison of hyd_1 HT and hyd_2 RT Series. *5.1.1. Evolution of the Individual Cs/uc Populations versus Total Water Loadings.* Figures 8 and 10 show the evolution of the individual Cs/uc populations as a function of total water molecules/uc contents. The Cs populations are evidently highly temperature dependent. In the hyd_1 HT series, the evolutions of the individual Cs/uc as a function of total Cs/uc in the 0 < water/uc < 28 range are as follows: Cs1/uc increases from 2.35 to 2.79, Cs2/uc increases from 2.74 to 3.40, and Cs3/uc

TABLE 7: Unit-Cell Parameters (Å), Ellipticities (ϵ), and $R(F^2)$% in the hyd_1 HT Series

T (°C)	a	b	c	ϵ	$R(F^2)$%
28	20.0592(2)	19.9411(2)	13.4300(1)	1.164	8.6
50	20.0553(2)	19.9457(2)	13.4260(1)	1.179	7.6
100	20.0498(2)	19.9465(2)	13.4217(1)	1.182	8.3
150	20.0496(2)	19.9455(2)	13.4173(1)	1.145	7.2
200	20.0583(2)	19.9456(2)	13.4130(1)	1.130	7.4
250	20.0698(2)	19.9443(2)	13.4111(1)	1.120	6.1
300	20.0792(2)	19.9437(2)	13.4106(1)	1.088	6.7
375	20.0853(2)	19.9395(2)	13.4085(1)	1.076	6.7
450	20.0861(2)	19.9381(2)	13.4069(1)	1.065	4.6[a]

[a] Values from ref 1.

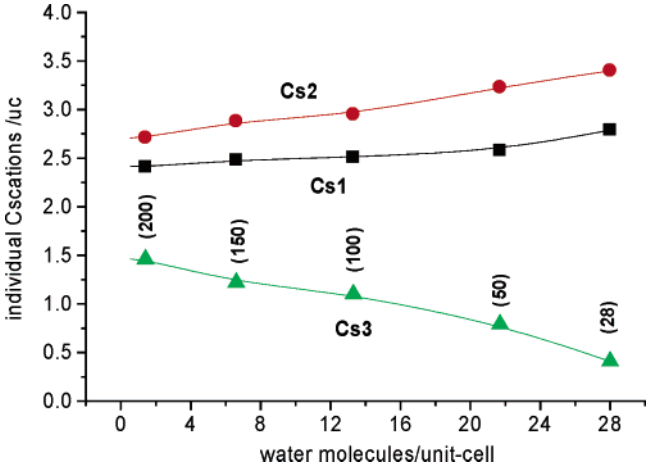

Figure 8. Populations of the Cs sites vs temperature of the individual Cs/uc concentrations versus total water/uc loadings in the hyd_1HT series. The values in parentheses correspond to the sample temperature. Total Cs/uc = 6.6.

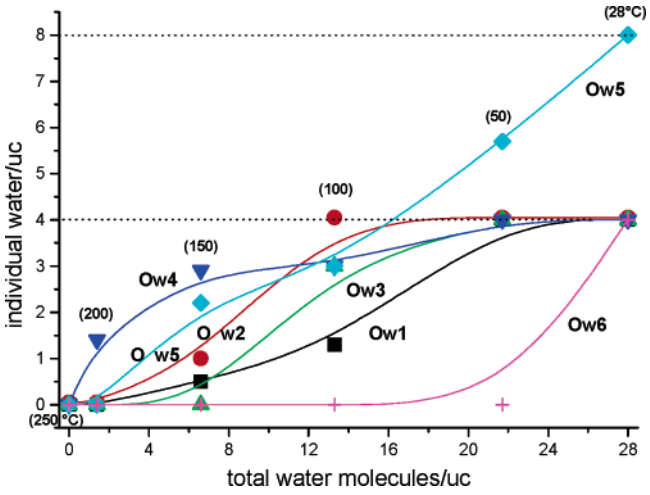

Figure 9. Populations of the individual water molecules/uc vs total water/uc at increasing temperatures (the hyd_1 HT series).

decreases drastically from 1.53 to 0.41 (a 373% decrease). In the hyd_2 RT series Cs1/uc increases from 2.61 to 3.52 (at 50% hydration) and then decreases from 3.52 to 2.73; Cs2/uc decreases from 2.66 to 2.25 (at 50% hydration) and then increases from 2.25 to 3.58, whereas Cs3/uc decreases steadily from 1.33 to 0.53 (a 251% decrease). In the hyd_2 RT series, the unexpected inversion in the Cs1/uc and Cs2/uc curves (close to 14 water/uc at ~50% hydration) is obviously related to the complexity of the investigated hydration mechanism (see the following section). In both series, the Cs3/uc contents decrease dramatically with increasing water fillings. It seems that the

TABLE 8: Individual Cation and Water Populations (uc) in the hyd_2 RT Series[a]

T_1	T_2	Cs1	Cs2	Cs3	total water	Ow1	Ow2	Ow3	Ow4	Ow5	Ow6	y(Cs2)
26	26	2.73	3.34	0.53	28	4	4	4	4	8	4	0.1438(3)
45	34	2.48	3.58	0.54	25.5	4	4	4	4	7.5	2	0.1475(3)
63	40	2.60	3.44	0.55	24.1	4	4	4	4	6.9	1.2	0.1463(3)
85	50	2.84	3.12	0.63	21.8	3.6	4	4	4	6.2	0	0.1438(3)
109	67	3.06	2.88	0.66	18.6	1.8	4	4	3.3	5.5	0	0.1422(3)
136	100	3.52	2.25	0.83	13.7	0.3	2.6	4	2.0	4.8	0	0.1307(3)
176	150	3.07	2.50	1.02	10.0	0	1.0	3.8	1.0	4.2	0	0.1017(3)
225	164	2.90	2.60	1.10	5.2	0	0	2.1	1.0	3.1	0	0.0899(3)
281	178	2.78	2.68	1.14	3.0	0	0	0.5	0.5	2.0	0	0.0891(3)
28	28	2.61	2.66	1.33	0							0.0586(3)[b]

[a] T_1 is the temperature of the heated sample before sealing (Experimental Section). T_2 is the actual equivalent temperature at which the sample has been heated (interpolation from the TG curve in Figure 1). Temperatures are give in °C. [b] From ref 1.

TABLE 9: Unit-Cell Parameters (Å), Ellipticities (ϵ), and $R(F^2)$% in the hyd_2 RT Series (at 26 °C)

T_2[a] (°C)	a	b	c	ϵ	$R(F^2)$%
26	20.0596(2)	19.9415(2)	13.4303(1)	1.164	7.5
34	20.0661(2)	19.9387(2)	13.4328(1)	1.150	9.7
40	20.0571(2)	19.9371(2)	13.4288(1)	1.182	7.0
50	20.0408(2)	19.9369(2)	13.4201(1)	1.189	6.5
67	20.0274(2)	19.9364(2)	13.4146(1)	1.216	6.7
100	20.0035(2)	19.9285(2)	13.4038(1)	1.223	7.8
150	20.0007(2)	19.9287(2)	13.4004(1)	1.230	8.2
164	19.9915(2)	19.9330(2)	13.3892(1)	1.211	6.8
178	19.9868(2)	19.9322(2)	13.3857(1)	1.215	6.7
28	19.9933(3)	19.9367(2)	13.3873(2)	1.218	4.6[b]

[a] See Table 8 for this equivalent temperature. [b] From ref 1.

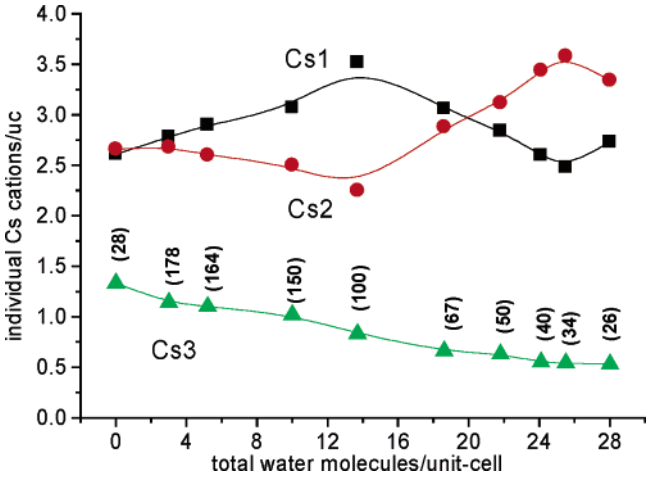

Figure 10. Population of the Cs sites vs temperature of the individual Cs/uc concentrations versus total water/uc loadings in the hyd_2 RT (26 °C) series. The values in parentheses correspond to equivalent temperatures interpolated from the TG curve in Figure 1 (section 3.1). Total Cs/uc = 6.6.

Ow6 molecule, which appears only at the end of the hydration process (at ~22 water/uc, 79% hydration), partially displaces the Cs3 cation from its site, triggering a cation relocation toward the more populated Cs1 and Cs2 locations.

5.1.2. Evolution of the Individual Water/uc Populations versus Total Water Loadings. Figures 9 and 11 depict the evolution of the individual water/uc populations versus total water/uc fillings. These figures clearly show that at lower water loads the hydration mechanisms in both hyd_1 HT and hyd_2 RT series are strikingly different. To the best of our knowledge, the present work is the first example that unmistakably reveals the drastic influence of the measurement environment on results

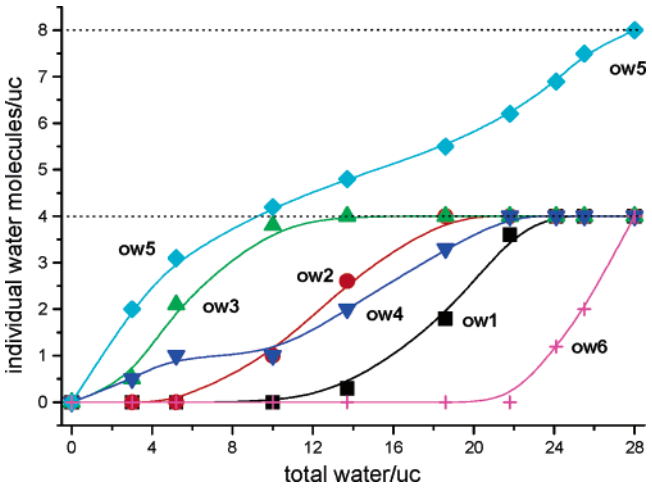

Figure 11. Populations of the individual water molecules/uc vs total water/uc at room temperature (the hyd_2 RT series).

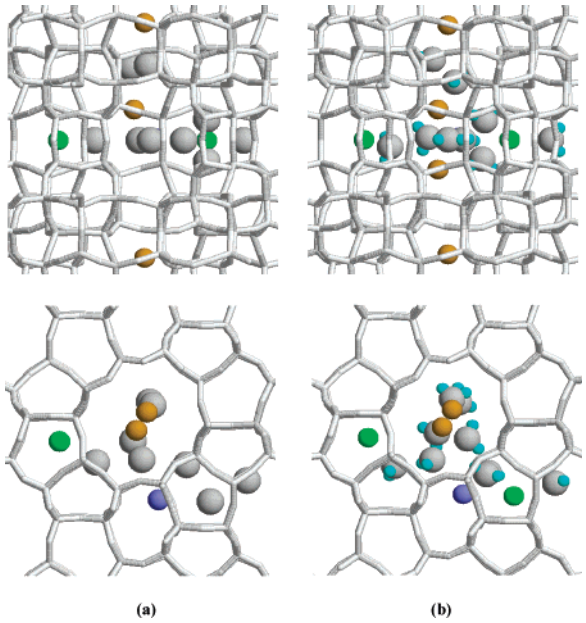

Figure 12. Comparison of the Cs locations (a) obtained by structure refinements and (b) by computer simulations. Upper drawings: Projection down the [001] direction—for the sake of clarity, only half of the Cs and water sites in the straight channel are represented. Lower drawings: Projection down the [010] direction.

TABLE 10: Atomic Coordinates of the Simulated Water Molecules in a Cationless MFI Framework

atom	*x*	*y*	*z*	occ/uc	site location[a]
Ow1	0.168	0.313	0.819	8	IIa
Ow2	0.039	0.245	0.882	4	I−IIa
Ow3	0.034	0.259	0.423	4	Ia
Ow4	-0.063	0.175	0.551	8	I−III
Ow5	0.343	0.250	0.855	4	I−IIb
Ow6	0.015	0.078	0.471	8	III
Ow7	0.053	0.248	0.633	4	Ib
Ow8	-0.064	0.225	0.729	4	Ic
Ow9	0.188	0.239	0.982	4	IIb

[a] Sites I/II and III for the intersection, the zigzag channel, and the straight channel, respectively. I−II and I−III are intermediate sites. Ia, Ib, and Ic are three sites located in the channel intersection.

from structural determinations of hydration mechanisms. Although the hyd_2 RT series does not correspond to an actual rehydration process, it can be assumed that this series is much closer to such a process than the hyd_1 HT series. By

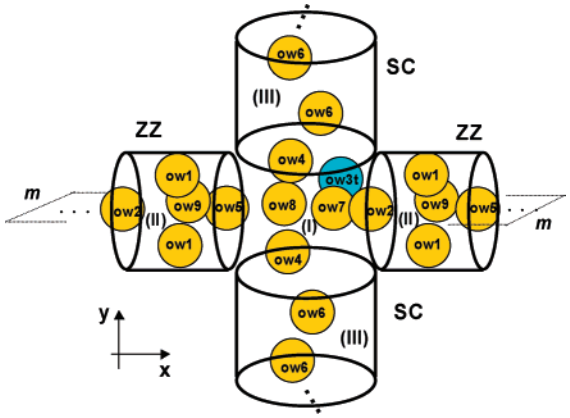

Figure 13. Schematic view of the locations of the nine independent water molecules in a hypothetical MFI-type material crystallizing with the framework structure corresponding to a strictly cationless $Cs_{6.6}H_{0.3}$-MFI zeolite.

comparison of the $Cs(H_2O)_n$ and $(H_2O)_4$ clusters mentioned in section 3.1 with the data reported in Figures 5 and 10 and in Table 9, hydration of the $Cs_{6.6}H_{0.3}$MFI·$28H_2O$ phase proceeds as shown in Table 11. According to this mechanism, it is not unlikely that in the actual hydration process (presumably also for rehydration) the very first $Cs2(H_2O)_2$ cluster forms in the straight channel sections, which explains why these channels deform elliptically already in the first hydration steps (Tables 8 and 9). With increasing water/uc load, the Cs2 cation becomes progressively hydrated and forms a complete cluster series, ranging from $Cs2(H_2O)_2$ to $Cs2(H_2O)_5$. In the last cluster, three water molecules belong to the first coordination sphere (Ow1, Ow3, Ow5), while the two remaining water molecules belong to the second sphere (Ow2, Ow5′; Table 5). During this hydration step, Cs2 migrates along the *b*-axis direction, its *y*-coordinate increasing from $y = 0.089$ to $y = 0.148$ (Table 8), which corresponds to a ∼1.2 Å displacement toward the center of the intersection (site I). The Cs1 and Cs3 cations do not migrate appreciably. At complete hydration the straight channel pore openings are significantly elliptical ($1.15 < \epsilon < 1.23$). This unusual structural response of the framework has already been observed in MFI/sorbate complexes, where sorbed species were located in or close to the straight channel[30] (sorbate-induced deformation). The formation of water clusters in MFI-type materials has already been advanced. In a temperature-programmed desorption experiment of a H−ZSM-5 (Si/Al = 13) zeolite, it was suggested that dimeric $(H_2O)_2$ and tetrameric $(H_2O)_4$ water clusters were formed.[31] Another study suggested that water and protons form neutral and ion-pair complexes in H−ZSM-5 phases.[32] Although, in the present work, the exchanged cation is Cs^+ (rather than a proton), our results support some of the hypotheses reported in refs 27 and 28, especially in what concerns the formation of a $(H_2O)_4$ tetramer located in the zigzag channel, with possible water−water and/or water−framework oxygen hydrogen bonds (Table 5).

5.2. Maximum Possible Water Loading in H-MFI: The Crystal Structure of $H_{6.9}$MFI·$38H_2O$. The water sorption capacities of the Cs-exchanged $Cs_{6.6}H_{0.3}$MFI phase and of its hypothetical cationless analogue are 28 (section 3.1) and 48 H_2O/uc (section 4), respectively. This implies that a Cs^+ cation occupies the same space as ∼3 water molecules. A similar answer (∼2.3) can be obtained when one computes the cation/water volume ratio from the kinetic volumes of the Cs^+ cation and of the water molecule, which are close to 21 and 9 $Å^3$, respectively. Does this mean that a water content higher than 28 H_2O/uc can be attained in an H-MFI material? To find out

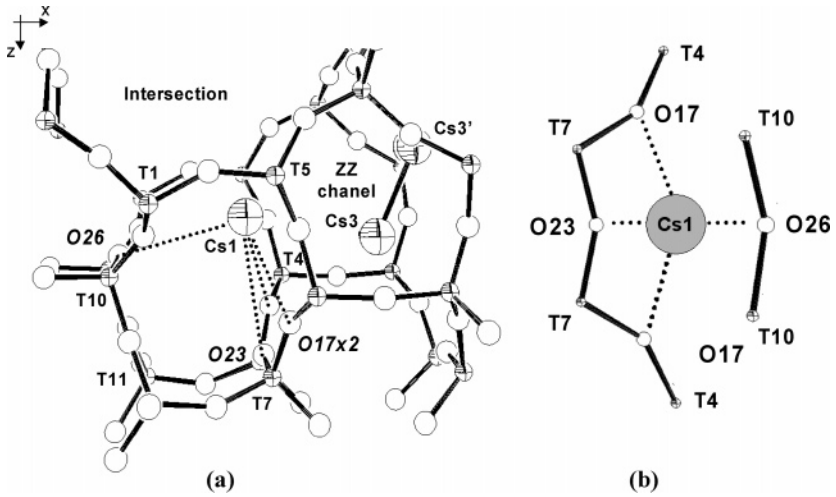

Figure 14. A potential acid site in ZSM-5, environment of the Cs1 cation in both (a) hydrated $Cs_{6.6}H_{0.3}MFI\cdot 28H_2O$ and (b) dehydrated $Cs_{6.6}H_{0.3}$-MFI (ref 1) phases.

TABLE 11: $Cs(H_2O)_n$ and $(H_2O)_n$ Clusters Appearing during the Hydration Process of $Cs_{6.6}H_{0.3}$MFI at Room Temperature (26 °C)

water/uc range	$Cs(H_2O)_n$ and $(H_2O)_4$ clusters
0−5.2	$Cs2(H_2O)_2 + Cs1(H_2O) + Cs3(H_2O)$
5.2−10	$Cs2(H_2O)_3 + Cs1(H_2O) + Cs3(H_2O)$
10−13.7	$Cs2(H_2O)_4 + Cs1(H_2O)_2 + Cs3(H_2O)_2$
13.7−21.8	$Cs2(H_2O)_5 + Cs1(H_2O)_2 + Cs3(H_2O)_2$
21.8−28	$Cs2(H_2O)_5 + Cs1(H_2O)_4 + Cs3(H_2O)_3 + (H_2O)_4$

the maximum possible water content—experimentally—we calcined the totally ammonium-exchanged parent $Na_{6.9}$MFI zeolite. The resulting H-MFI phase was shown to adsorb 38 H_2O/uc as determined from the thermogravimetric dehydration curve and the water uptake isotherm at normal pressure and temperature. This is rather far from the theoretically simulated 48 H_2O/uc value. If we estimate the kinetic volume of a proton to be about 1.61 Å^3 (a sphere of diameter 1.45 Å), then the 6.9 protons occupy a volume of about $(6.9 \times 1.61)/9 \approx 1.2$ water molecules. For this reason, the protons are definitely not responsible for the apparent loss in the water sorption capacity. With seven independent water molecules, simulated and experimental, thermogravimetric H_2O/uc saturation capacities are very close. The structural refinement of the $H_{6.9}MFI\cdot 38H_2O$ crystal structure gives a slightly different value, namely, 42(2) H_2O/uc: The refined populations for the seven Ow1/Ow2/Ow3/Ow4/Ow5/Ow6/Ow7 water species are 3.8(2)/4.7(2)/2.1(2)/11.4(4)/5.9(2)/8.7(2)/5.7(2), respectively. Given that the maximum population of a water species close to the *m* mirror plane ($y \approx {}^1/_4$ in the *Pnma* space group) is 4/uc, some of the refined populations must be constrained to 4/uc or 8/uc. As a consequence, the total water content decreases to ∼36(2) H_2O/uc, which is very close to the thermogravimetric value. The difference between the refined and the crystallographically acceptable H_2O/uc values also stems from the facts that (1) the different water molecules are substantially disordered and (2) the locally stabilizing cation/water interactions are absent in the H-form zeolite. Some tables and figures corresponding to the structure refinement of the $H_{6.9}MFI\cdot 38H_2O$ phase are published in the Supporting Information.

5.3. Ellipticity of the D10R Channel Openings. In highly siliceous materials (silicalite, Si/Al > ∼150) the pore openings of the straight and/or zigzag channels become often markedly elliptical when extraframework aromatic molecules have been sorbed. In the case of cation-exchanged ZSM-5 materials, it is shown that in both the dehydrated and the hydrated $Cs_{6.6}H_{0.3}$-MFI phases the ellipticities of the straight channel D10R sections are also rather pronounced (Tables 7 and 9). Surprisingly, in $H_{6.9}MFI\cdot 38H_2O$ the ellipticity of the straight channel pore openings has almost vanished ($\epsilon = 1.079$), and this value is now close to that observed in a purely siliceous silicalite ($\epsilon =$ 1.077 and 1.071, monoclinic $P2_1/n\cdot 1\cdot 1$ framework symmetry).[33] This experimental result is remarkable for what it reveals. It points to the origin of the flexibility of the MFI-type framework, i.e., the presence of large cations (as in dehydrated Cs^+-exchanged MFI phases[1] or in Rb^+-, K^+-, and Tl^+-exchanged MFI phases[34]), of hydrated Cs cations (formation of $Cs(H_2O)_n$ clusters), or of tight-fitting organic sorbates (e.g., benzene,[35] *p*-xylene,[36] or *p*-nitroaniline[37]) in or close to the straight channel 10-ring pore openings.[30] Data reported in Tables 7 and 9 and in Table 8 of ref 1 support this claim convincingly. Although in hydrated Cs-exchanged MFI-type materials ellipticity seemingly decreases as dehydration progresses (Table 7, hyd_1 HT series at increasing temperatures), this decrease is due entirely to thermal expansion of the framework. In progressively dehydrated Cs-exchanged MFI material (hyd_2 RT series), measured at ambient temperature, the ellipticity actually increases to the value cited in ref 1, as the Cs cations shed their hydration shell (Table 9).

Knowledge concerning the possible presence of elliptical straight and/or zigzag channel pore openings in MFI-type host−guest complexes is of paramount importance for predicting the possible location(s) of extraframework species. This knowledge can be obtained at the earlier stages of a structure refinement.[38,39] For instance, (1) in the silicalite/4CCl_4 complex,[30] no channel deformations are observed, and the molecule resides at the channel intersection (site I), (2) in the silicalite/4*p*-xylene[11,38] and silicalite/8benzene[35] complexes only the straight channel sections (site III) are elliptical, and the molecules reside in (4 of the 8 benzene molecules/uc) or interact through (infinite polymeric *p*-xylene···*p*-xylene chains) the straight channels, (3) in the silicalite/8*p*-xylene complex[36] both D10R channel sections are elliptical, and the molecules reside or interact in both channel sections (4 *p*-xylene/uc in site II and 4/uc in site III), and (4) in the silicalite/6benzene complex[35] only the zigzag channels are elliptical: Two of the six benzene molecules reside in the zigzag channel sections (site II). All of this again underscores the importance of having reliable and accurate crystal structural information prior to carrying out any sensible computer simulation. A good case in point is the as-synthesized ZSM-5/4tripropylbenzylammonium (P3BZY) complex. Given that the

templating molecule (the structure-directing tripropylbenzylammonium ion) adopts several conformations in the MFI-type framework, it is indispensable—before attempting any computer simulation—to know where the terminal aromatic C_6H_5 ring is likely to reside. A partial structure refinement of the framework structure in the ZSM-5/4P3BZY crystal (see ref 1 in the Cs^+ cation case) shows that only the straight channel 10-ring pore openings are significantly elliptical[39] ($\epsilon = 1.134$). Accordingly we expect the aromatic ring to be located in the straight channel sections.

6. Conclusions

The present work is the first instance of a successful determination of the dehydration mechanism in a hydrated, cation-exchanged $Cs_{6.6}H_{0.3}MFI{\cdot}28H_2O$ zeolite from X-ray powder diffraction pattern refinements. Some of the questions raised in the Introduction have now an answer:

(1) *Where are the Cs atoms located and what are their relative populations for $C_{6.6}$MFI phases, both hydrated and dehydrated?* We believe that we have been able to determine successfully both locations and populations of the Cs cations in a $C_{6.6}$MFI material.

(2) *Have we been able to do this for all degrees of cation exchange?* Presently, we have only been able to do this in the case of the completely dehydrated $C_{6.6}$MFI phases (ref 1). The results concerning the hydrated Cs_xMFI phases for the $0.7 < x < 7.7$ Cs/uc contents will be reported in a forthcoming study.[40]

(3) *Are these Cs and H_2O locations and populations similar in the hydrated, in the dehydrated, or in rehydrated phases?* This question is partially answered in the present work; the definitive answer will be given elsewhere.[40]

(4) *What is the influence of temperature?* The Cs and water distributions depend strikingly on the measurement protocol, i.e., whether the diffraction measurements have been carried out in or ex situ. The complete dehydration mechanism is much easier to establish in the case of the hyd_2 RT series. Increasing temperatures provoke substantial cation and sorbate movements, which have to be investigated for each particular zeolitic host/guest system.

(5) *Where do the cations relocate to in the presence of sorbed polar molecules?* The relocations of the Cs^+ cations are controlled by both the temperature and the sorbed species (H_2O in our case). The Cs2 cation in the hydrated phases moves toward the center of the intersection.

(6) *Which are the migrating species: the cations, the sorbents, or both?* During the dehydration process, the answer is both. Nevertheless, only some cations move substantially. In the present work, it seems that the most mobile cation is Cs2. This cationic species is the one most involved in the overall hydration process. During the progressive hydration, this cation yields successively the $Cs2(H_2O)_2$, $Cs2(H_2O)_3$, $Cs2(H_2O)_4$, and $Cs2(H_2O)_5$ clusters. The Cs1/uc and Cs2/uc populations increase progressively, while the Cs3/uc populations steadily decrease (in the ~3/1 ratio). These results clearly show that in the case of the progressive absorption of a polar water molecule the cationic movements are mostly restricted to partial jumps (or relocations) between the three Cs^+ sites, while some of their relative populations may drastically change. Other examples, illustrating such cation relocations in other microporous materials, are observed in some (Cs,Na)-exchanged Y[41a,b] and X[41c] or in NaY[42] faujasite-type zeolites, where the I′, II′, II, III, and rarely I sites are mostly involved. Neither any continuous long distance cation migration (as, for instance, a cation migrating smoothly from a zigzag channel location toward the center of a channel intersection, a travel of nearly 6 Å) nor any merging of cation positions on a single site are observed (as mostly supposed in many theoretical simulations—see ref 43 and references therein).

(7) *Do the locations of the extraframework species depend on the measuring conditions?* The answer is definitely yes. Concerning the dehydration and the hydration, this is illustrated by the structural evolutions of the cations and the water molecules in the hyd_1 HT and hyd_2 RT series. The answer to the third possibility, i.e., a hyd_3 RT series corresponding to progressively rehydrated samples at room temperature, is not yet available. Investigation of such a rehydration process, which is presently planned, is the only one strictly comparable to experimental results obtained from hydration isotherms or high-precision differential molar absorption calorimetry.[44,45]

(8) *Is it possible to predict the locations of the sorbed water molecules by computer simulations?* Crystal structure investigations yield the positions of extraframework species from experimental data on real materials. They thus deliver the structural model closest to reality. Theoretical computer simulations, nevertheless, also have their raison d'être; they fill in the gaps where there is no experimental data, and they also often generate sound starting refinement models for guest positions in the cavities, even in complex host−guest zeolitic systems. In the present work, we have shown that the positions of water molecules in the hydrated phases are rather sensibly predicted.

(9) *How is the framework symmetry and/or its flexibility affected by the cations and/or the nature of the sorbed molecules?* In our opinion, this is a point that will never be thoroughly predicted by computer simulations. One of the major obstacles is the widely observed existence of multiphase domains in MFI/sorbate systems, as, for instance, in the silicalite/*p*-xylene system for $0 < p$-xylene/uc < 2 and $4 < p$-xylene/uc < 8 loadings.[46−48] And so the only possible way to obtain an unambiguous answer concerning the flexibility of an MFI-type framework is a crystal structure determination. Theoretical work deals usually only with short-range and/or local atomic relaxations in some restricted cluster-type framework moeities, focusing on specific interaction centers (e.g., cation, proton, Si−OH silanol group, or double bond). Furthermore, in most theoretical investigations, the MFI-type structure model used seldom corresponds to an actual framework symmetry—for lack of reliable experimental structural data. This unfortunate state of affairs explains the overabundance of theoretical work compared to experimental structural studies (e.g., 183 simulations versus 12 experimental studies reported in ref 43) and why most of the computer simulations converge toward awkward (for instance, a $(C_6H_6)_2$ cluster located in the channel intersection of silicalite) or erroneous solutions (among others sorption at lower fillings of benzene in the zigzag channels or sorption of linear alkanes in silicalite).

Extension of our work to dehydrated and hydrated Na^+-, K^+-, Rb^+-, Ba^{2+}-, and Cu^{2+}-exchanged MFI-type zeolites and to NaY, BaY, or BaX phases (FAU-type materials) will show if some of the conclusions mentioned above are valid generally or are applicable only to some particular cases.

Acknowledgment. We thank the staff of the Swiss−Norwegian Beam Lines for assistance. H.P.W. thanks the Swiss National Science Foundation for steadfast support and the Tisserand Foundation, Montricher, for a fellowship.

Supporting Information Available: Tables and figures for the $H_{6.9}MFI{\cdot}38H_2O$ phase: atomic framework coordinates, ORTEP drawing, and principal water−framework oxygen and

water−water distances. This material is available free of charge via the Internet at http://pubs.acs.org.

References and Notes

(1) Mentzen, B. F.; Bergeret, G.; Emerich, H.; Weber, H.-P. *J. Phys. Chem. B* **2006**, *110*, 97−106.

(2) Park, S.-H.; Liu, H.; Kleinsorge, M.; Grey, C. P.; Toby, B. H.; Parise, J. B. *Chem. Mater.* **2004**, *16*, 2605−2614.

(3) (a) Baerlocher, Ch.; Meier, W. M.; Olson, D. H. *Atlas of Zeolite Framework Types*, 5th ed.; Elsevier: Amsterdam, 2001. (b) Mobil Oil Corp. Neth. Patent 7,014,807, 1971. (c) Kokotailo, G. T.; Lawton, S. L.; Olson, D. H.; Meier, W. M. *Nature* **1978**, *272*, 437−438. (d) Olson, D. H.; Kokotailo, G. T.; Lawton, S. L.; Meier, W. M. *J. Phys. Chem.* **1981**, *85*, 2238−2243.

(4) Ohgushi, T.; Niwa, T.; Araki, H.; Ichino, S. *Microporous Mater.* **1997**, *8*, 231−239.

(5) Spackman, M.; Weber, H. P. *J. Phys. Chem.* **1988**, *92*, 794−796.

(6) Mortier, W. J. *Compilation of Extra Framework Sites in Zeolites*; Butterworth Scientific Limited: Guildford, U.K., 1982; pp 19−31 for FAU and pp 41−48 for LTA.

(7) Zhenyl, L.; Wangjin, Z.; Qin, Y.; Guanglie, L.; Wangrong, L.; Shunju, W.; Youshi, Z.; Bingxiong, L. In *Proceedings of the 7th International Zeolite Conference*; Kodansha Elsevier: Tokyo, Japan, 1986; pp 415−422.

(8) Lin, J. C.; Chao, K.-J.; Wang, Y. *Zeolites* **1991**, *11*, 376−379.

(9) Huddersman, K. D.; Rees, L. V. C. *Zeolites* **1991**, *11*, 270−176.

(10) Mentzen, B. F.; Sacerdote-Peronnet, M.; Bouix, J. *C. R. Acad. Sci., Ser. II* **1992**, *315*, 1073−1078.

(11) Mentzen, B. F.; Gélin, P. *Mater. Res. Bull.* **1998**, *33*, 109−116.

(12) Olson, D. H.; Khosrovani, N.; Peters, A. W.; Toby, B. H. *J. Phys. Chem. B* **2000**, *104*, 4844−4848.

(13) Grau-Crespo, R.; Peralta, A. G.; Ruiz-Salvador, A. R.; Gómez, A.; López-Cordero, R. *Phys. Chem. Chem. Phys.* **2000**, *2*, 5716−5722.

(14) Beerdsen, E.; Dubbeldam, D.; Smit, B.; Vlugt, T. J. H.; Calero, S. *J. Phys. Chem. B* **2003**, *107*, 12088−12096.

(15) Esemann, H.; Förster, H.; Geidel, E.; Krause, K. *Microporous Mater.* **1996**, *6*, 321−329.

(16) Miyamoto, A.; Matsuba, K.; Kubo, M.; Kawamura, K.; Inui, T. *Chem. Lett.* **1991**, 2055−2058.

(17) Wu, P.; Ma, Y. H. In *Proceedings of the 6th International Zeolite Conference*, Reno, NV, July 10−15, 1984; Olson, D. H., Bisio, A., Eds.; Butterworths: Guildford, U.K., 1984; pp 251−260.

(18) Moissette, A.; Marquis, S.; Gener, I.; Brémard, C. *Phys. Chem. Chem. Phys.* **2002**, *4*, 5690−5696.

(19) Moissette, A.; Brémard, C. *Microporous Mesoporous Mater.* **2001**, *47*, 345−357.

(20) Wiles, D. B.; Young, R. A. *J. Appl. Crystallogr.* **1981**, *14*, 149−151.

(21) Toby, B. H. EXPGUI, a graphical user interface for GSAS. *J. Appl. Crystallogr.* **2001**, *34*, 210−213.

(22) Caldwell, J. W.; Kollman, P. A. *J. Phys. Chem.* **1995**, *99*, 6208−6219.

(23) Eroshenko, V.; Regis, R.-C.; Soulard, M.; Patarin, J. *J. Am. Chem. Soc.* **2001**, *123*, 8129−8130.

(24) Eroshenko, V.; Regis, R.-C.; Soulard, M.; Patarin, J. *C. R. Phys.* **2002**, *3*, 111−119.

(25) Olson, D. H.; Zygmunt, S. A.; Erhardt, M. K.; Curtiss, L. A.; Iton, L. E. *Zeolites* **1997**, *18*, 347−349.

(26) Desbiens, N.; Boutin, A.; Demachy, I. *J. Phys. Chem. B* **2005**, *109*, 24071−24076.

(27) Nachtigallova, D.; Nachtigall, P.; Sauer, J. *Phys. Chem. Chem. Phys.* **2001**, *3*, 1552−1559.

(28) Jungsuttiwong, S.; Khongpracha, P.; Truong, T. N.; Limtrakul, J. Proceedings of the 13th International Zeolite Conference, Montpellier, France. *Stud. Surf Sci. Catal.* **2001**, *135*, 2518.

(29) Nachtigallova, D.; Nachtigall, P.; Sierka, M.; Sauer, J. *Phys. Chem. Chem. Phys.* **1999**, *1*, 2019−2026.

(30) Mentzen, B. F. *Mater. Res. Bull.* **1992**, *27*, 831−838.

(31) Olson, D. H.; Haag, W. O.; Borghard, W. S. *Microporous Mesoporous Mater.* **2000**, *35*−*36*, 435−446.

(32) Zygmunt, S. A.; Curtiss, L. A.; Iton, L. E. *J. Phys. Chem. B* **2001**, *105*, 3034−3038.

(33) van Koningsveld, H.; Jansen, H.; van Bekkum, H. *Zeolites* **1990**, *10*, 235−241.

(34) Mentzen, B. F., et al., in preparation.

(35) Mentzen, B. F.; Lefèbvre, F. *Mater. Res. Bull.* **1997**, *32*, 813−821.

(36) van Koningsveld, H.; Tuinstra, F.; van Bekkum, H.; Jansen, J. C. *Acta Crystallogr., Sect. B* **1989**, *45*, 423−431.

(37) Mentzen, B. F.; Lefèbvre, F. *J. Chim. Phys.* **1998**, *95*, 1052−1067.

(38) Mentzen, B. F.; Lefèbvre, F. *Mater. Res. Bull.* **1995**, *30*, 613−620.

(39) Mentzen, B. F.; Tuel, A.; Bayard, F. *Microporous Mesoporous Mater.*, in press.

(40) Mentzen, B. F., et al., in preparation.

(41) (a) Norby, P.; Poshni, F. I.; Gualtieri, A. F.; Hanson, J. C.; Grey, C. P. *J. Phys. Chem. B* **1998**, *102*, 839−856. (b) Koller, H.; Burger, B.; Schneider; A. M.; Engelhardt, G.; Weitkamp, J. *Microporous Mater.* **1995**, *5*, 219−232. (c) Lima, E. J.; Ibarra, I. A.; Vera, M. A.; Lara, V. H.; Bosch, P.; Bulbulian, S. *J. Phys. Chem. B* **2004**, *108*, 12103−12110.

(42) Grey, C. P.; Poshni, F. I.; Gualtieri, A. F.; Norby, P.; Hanson, J. C.; Corbin, D. R. *J. Am. Chem. Soc.* **1997**, *119*, 1981−1989.

(43) van de Graaf, B.; Njo, S. L.; Smirnov, K. S. Introduction to Zeolite Modeling. In *Reviews in Computational Chemistry*; Lipkowitz, K. B., Boyd, D. B., Eds.; John Wiley and Sons: New York, 2000; Vol. 14, pp 137−223.

(44) Boddenberg, B.; Rakhmatkariev, G. U.; Viets, J. *Ber. Bunsen-Ges. Phys. Chem.* **1998**, *102*, 177−182.

(45) Boddenberg, B.; Rakhmatkariev, G. U.; Greth, R. *J. Phys. Chem. B* **1997**, *101*, 1634−1640.

(46) Mentzen, B. F.; Védrine, J. *C. R. Acad. Sci., Ser. II* **1985**, *301*, 1017−1020.

(47) Mentzen, B. F. *J. Appl. Crystallogr.* **1988**, *21*, 266−271.

(48) Fyfe, C. A.; Strobl, H.; Kokotailo, G. T.; Kennedy, G. J.; Barlow, G. E. *J. Am. Chem. Soc.* **1988**, *110*, 3373−3380.